Journal of Materials Chemistry

Dynamic Article Links

Cite this: *J. Mater. Chem.*, 2012, **22**, 6851

www.rsc.org/materials

PAPER

Enhanced catalytic activity induced by defects in mesoporous ceria nanotubes†

Guomin Hua, Lide Zhang,* Guangtao Fei and Ming Fang

Received 29th July 2011, Accepted 9th December 2011
DOI: 10.1039/c2jm13610d

Mesoporous ceria nanotubes are fabricated by the following process: ceria was deposited on the surface of ZnO nanorods by the ultrasonic assisted successive ionic layer adsorption and reaction (SILAR) method to obtain ceria/ZnO composite nanostructures, then, the ZnO core was removed by HNO_3 solution, resulting in the formation of ceria nanotubes, which have the large surface area of 109 $m^2\ g^{-1}$. Such ceria nanotubes have excellent catalytic performance in the CO → CO_2 conversion, and the reaction start temperature is about 100 °C lower than that of commercial ceria (CeO_2) particles. The specific catalytic activity of the ceria nanotubes is 9 times higher than that of commercial ceria particles at 320 °C. The XPS and Raman investigations have proved that the Ce^{3+} ion number in the surfaces is about 23% of total cerium ion number, which may be responsible for the high reduction performance to oxygen. The positron annihilation experiments prove that a large amount of vacancies and vacancy groups exist in these samples. A large amount Ce^{3+} formation is closely associated with these vacancies and vacancy groups. Temperature programmed reduction (H_2-TPR) experiments further confirm that the enhanced activity of mesoporous ceria is in contrast to commercial ceria particles. Moreover, for ceria nanotubes the enhanced activity is attributed to enhancement of the surface activity caused by Ce^{3+} ions. The catalysis activity stability arises from contribution of the cycle transition between Ce^{3+} and Ce^{4+} ions.

1. Introduction

Ceria as an important catalyst has been well recognized, and it has been widely used in various application fields, such as purification of exhaust gases in three-way automotive catalytic converters,[1] solid oxide fuel cells,[2,3] antioxidant in biomedicine,[4–6] and many other catalytic applications.[7–9] Understanding the origin and mechanism of the catalytic activity of ceria, however, remains incomplete. The incomplete understanding is obviously a major barrier in broadening applications of ceria. Generally, the catalytic activity of ceria involves the transition between its two oxidation states: Ce^{3+} ↔ Ce^{4+}; and as such, catalytic activity is limited by the transition from Ce^{4+} to Ce^{3+} at low temperature and low active site density.[10,11] Recently, the origin and mechanism of catalytic activity of ceria have drawn significant attention, and many theoretical works have been reported.[12–16] Skorodumova *et al.*[12] theoretically suggested that oxygen-vacancy formation could induce valence transition of Ce ions in ceria from +4 to +3. This valence transition arises from oxygen escaping from lattice sites, leaving vacancy sites with two electrons at each vacancy. Single electron defects containing Ce^{3+} ions can serve as coordination sites to induce formation of active oxygen species.[17,18] Those investigations suggested that synthesizing nano-ceria with abundant oxygen vacancies and single electron defects of Ce^{3+} ions are effective routes for enhancing catalysis activity of ceria. Parker *et al.*[16] theoretically proposed a new polycrystalline multilayered ceria nanotube structure with high oxygen storage capabilities and reactivity, which is closely related to the vacancy cluster segregation behavior. Parker *et al.* also suggested that the nanotubes of ceria are very difficult to synthesize, and their surfaces are very difficult characterize.

In the work of this paper, we synthesized mesopores ceria nanotubes with increased amounts of oxygen vacancies and single electron defects containing Ce^{3+}. The concentration of Ce^{3+} in ceria nanotubes is elevated to 23% of the total Ce ions (Ce^{3+} + Ce^{4+} ions). Abundant oxygen vacancy clusters segregate in ceria nanotubes. The catalytic origin and mechanism of ceria nanotubes were investigated. The catalytic capacity of ceria nanotubes was examined in CO to CO_2 conversion. The examination showed that the mesoporous ceria nanotubes reduced the beginning temperature of the conversion from CO to CO_2 by about 100 °C compared to commercial ceria particles. The specific activity of mesoporous ceria nanotubes is 9 times that of commercial ceria particles at 320 °C.

Key Laboratory of Materials Physics, Anhui Key Laboratory of Nanomaterials and Nanostructure, Institute of Solid State Physics, Chinese Academy of Sciences, Hefei, 230031, P.R. China. E-mail: ldzhang@issp.ac.cn; Fax: +86-(0)551-5591434; Tel: +86-(0)551-5591420

† Electronic supplementary information (ESI) available. See DOI: 10.1039/c2jm13610d

2. Results and discussion

The transmission electron microscopy (TEM) image of nanostructured ceria is presented in Fig. 1a. The nanostructured ceria are in the form of nanotubes. The hollow pore size and wall thickness of each ceria nanotube are respectively about 25 nm and 6 nm. As shown in the high-resolution TEM image in Fig. 1b, the walls of the ceria nanotubes display a mesoporous structure. The selected area electron diffraction (SAED) pattern reveals that the mesoporous ceria nanotubes are polycrystalline. The structural features of mesoporous polycrystalline ceria nanotubes are observable in the high magnification HRTEM images in Fig. 1c and 1d. Steps and corners are formed on the surfaces of nanotubes. The exposed major facets are the {111} planes and {100} planes. More importantly, a high density of grain boundaries are observed. Additional information can be found in Fig. S1, S2 and S3 in the ESI.†

The nitrogen adsorption experiment indicates that the ceria nanotubes after calcinations at 500 °C possess a mesoporous structure (see ESI† Fig. S4); and the specific area is 109 $m^2\ g^{-1}$ calculated by the Brunauer–Emmett–Teller method. Comparing to the ordered mesoporous ceria and ceria nanowires reported in ref. 19 and 20, the surface area of the mesoporous ceria nanotube is significantly increased.

The X-ray photoelectron spectroscopy (XPS) spectra are shown in Fig. 2. The ratio of Ce^{3+} ions to Ce^{4+} ions in ceria nanotubes can be obtained as reported in ref. 21 and 22. The concentration of Ce^{3+} ions is elevated to 23% of the total cerium ions. But to the commercial ceria nanoparticles, this value is only 8%. The high concentration of Ce^{3+} ions in mesoporous polycrystalline ceria nanotubes leads to remarkable increment of forming negatively charged active oxygen species, as shown in the Raman scattering spectrum (see ESI† Fig. S5).

A basic rule that should be obeyed for a stable system is the electrostatic balance. Because a high percentage of negatively charged Ce^{3+} ions are observed in mesoporous ceria nanotubes, we assume that there should be a large amount of positively charged defects or impurities in it. Since no other impurities in the mesoporous ceria nanotubes are observed from the XPS spectrum, we think the defect of positively charged O vacancies

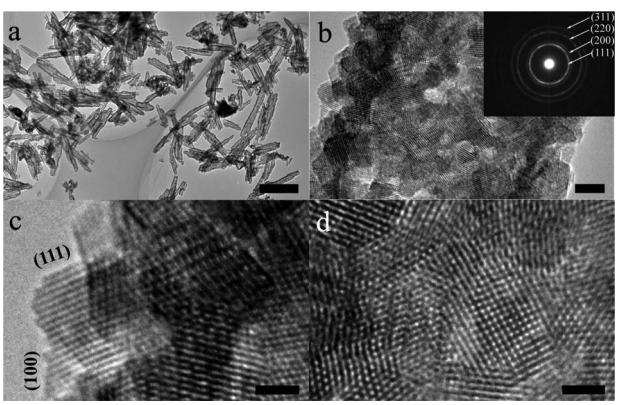

Fig. 1 The microstructure of mesoporous ceria nanotubes. (a) Low magnification TEM image, scale bar: 400 nm; (b) the high-resolution TEM image of mesoporous ceria nanotubes, scale bar: 5 nm, inset: the SAED pattern; (c) the high magnification images of the rough surface; (d) the high magnification image of nanotube wall. Scale bar: 2 nm in (c) and (d).

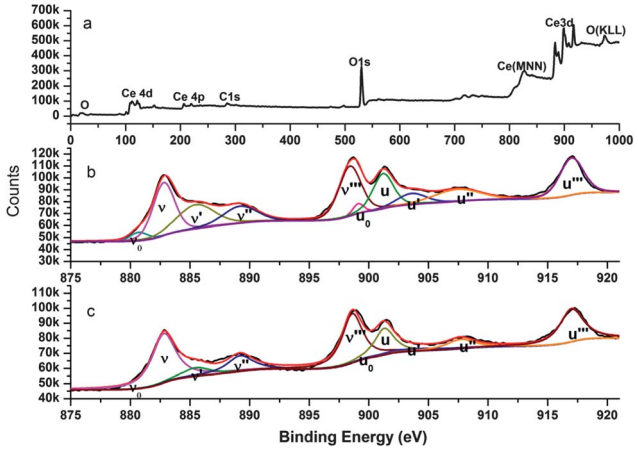

Fig. 2 The XPS spectra of mesoporous ceria nanotubes. (a) The survey spectrum, (b) the Ce 3d core level spectrum and fitting results, ν denotes Ce $3d_{5/2}$, u denotes Ce $3d_{3/2}$, where the fitting peaks of ν_0,ν′, u_0 and u′ belong to Ce^{3+} ions and fitting peaks of ν,ν″, ν‴, u, u″ and u‴ belong to Ce^{4+} ions, (c) the Ce 3d core level spectrum and fitting results of commercial ceria particles.

could be causing this electrostatic balance. To verify this assumption, the positron annihilation experiments provide more detailed information on oxygen vacancies in mesoporous polycrystalline ceria nanotubes.[23,24] Fig. 3a presents positron lifetime spectra of mesoporous ceria nanotubes and commercial ceria particles. Table 1 shows the fitting results of positron lifetime spectra. The results show that larger vacancies with positron

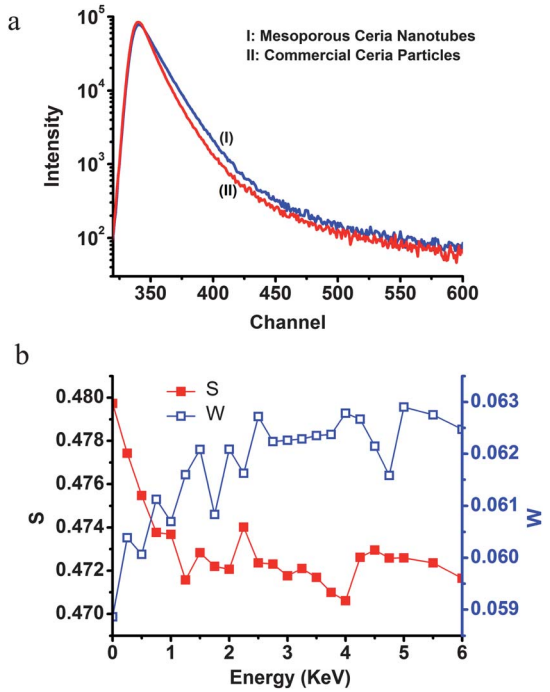

Fig. 3 (a) The positron lifetime spectra of mesoporous ceria nanotubes and commercial ceria particles as reference; (b) the Doppler broadening experiment results, the shape parameter of the Gaussian curve of the Doppler broadening spectrum is referred to as *S*, and the wing parameter of the Gaussian curve of the Doppler broadening spectrum is referred to as *W*.

lifetimes of 297 ps are dominant in the mesoporous polycrystalline ceria nanotubes. Those lifetimes are much longer than the positron annihilation lifetime of 201 ps in commercial ceria particles. In view of the higher thermodynamic barrier for the formation of large oxygen vacancies,[25,26] the existence of larger oxygen vacancies causes the formation energy (E_f) of large oxygen vacancies in the mesoporous ceria nanotubes to be lower than that of the commercial ceria particles.[27] The lower formation energy of large oxygen vacancies could effectively promote the reducibility by the process: $2Ce^{4+} + O^{2-} \rightarrow 2Ce^{3+} + \square + 1/2O_2$, where $\square$ represents an oxygen vacant site originating from the removal of O^{2-} from the surface lattice.[17] Moreover, as shown in Fig. 3b, the Doppler broadening experiment reveals that large oxygen vacancies are distributed on the surface of mesoporous ceria nanotubes, which is reflected by the decreasing *S*-parameter and the increasing *W*-parameter with the increase in the incident positron/ energy.[23,28]

Fig. 4a demonstrates the catalytic capacity of mesoporous ceria nanotubes in the oxidation of CO and is compared to commercial ceria particles. With commercial ceria particles, the CO to CO_2 conversion starts at 320 °C, and the catalytic efficiency increases slowly at higher temperature. With mesoporous ceria nanotubes, the entire conversion from CO to CO_2 is completed at 320 °C. The catalytic efficiency of the mesoporous ceria nanotubes increases rapidly at lower temperature, and the mesoporous ceria nanotubes reduced the conversion starting temperature by 100 °C, by comparing both catalysts at 320 °C. From the calculation of specific activity which is defined as the amount of CO converted on a unit surface area of the catalyst in a unit reaction duration, it is observed in Fig. 4b that the specific activity of the mesoporous ceria nanotubes is 9 times as high as that of the commercial ceria particles.

H_2-TPR profiles as shown in Fig. 5 provide further information on enhanced catalytic activity of mesoporous polycrystalline ceria nanotubes. Two H_2-consumption peaks in each profile can be observed. For mesoporous polycrystalline ceria nanotubes, the reduction peak located between 280–600 °C is substantially higher than that of commercial ceria particles, which means that the mesoporous polycrystalline ceria nanotubes possess stronger surface activity than that of the commercial ceria particles.[10] From the Raman scattering spectrum, great numbers of negatively charged active oxygen species induced by the one electron defects of Ce^{3+} ions exist on the surface, and are responsible for the enhanced surface activity. The enhanced catalytic mechanism can be suggested as follows:

$$Ce^{3+} + O_2 \rightarrow Ce^{4+} + O_2^-$$

$$Ce^{4+} + O_2^- + 2H_2 \rightarrow Ce^{3+} + 2H_2O$$

Table 1 The fitting results of positron lifetime spectra[a]

	τ_1(ps)	τ_2(ps)	τ_3(ns)	I_1 (%)	I_2 (%)	I_3 (%)
Ceria NT	297	475	2.387	69.1	29.8	1.1
Ceria RF	201	397	1.67	66.5	32.5	1

[a] Note: the mesoporous ceria nanotubes are referred to as ceria NT and the commercial ceria particles are referred to as ceria RF.

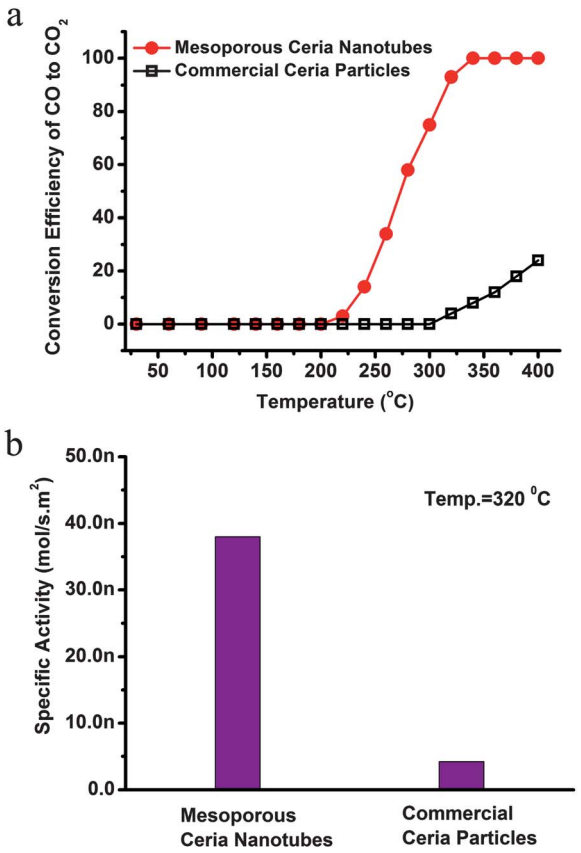

Fig. 4 The catalytic activity of CO to CO_2. (a) The conversion efficiency *vs.* temperature; (b) the specific activity of the mesoporous ceria nanotubes and the commercial ceria particles at 320 °C, the specific activity is defined as the amount of CO converted on a unit surface area of the catalyst in a unit reaction duration.

Mesoporous ceria nanotubes show unprecedented surface catalytic activity in the conversion CO → CO_2. In this work, we investigated the origin of high catalytic activity of mesoporous ceria nanotubes by analyzing the relationship of the catalytic activity with the change of cerium ion valence state and oxygen vacancy defects. The low oxygen vacancy formation energy in

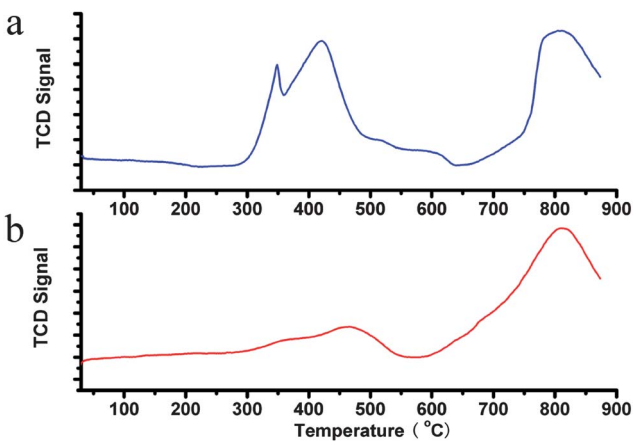

Fig. 5 H_2-TPR profiles reduced by the specific surface area. (a) Mesoporous ceria nanotubes; (b) commercial ceria particles.

mesoporous ceria nanotubes facilitates high concentrations of oxygen vacancy clusters on the surface of mesoporous polycrystalline ceria nanotubes. Consequently, the thermodynamic barrier for the reversible transition between Ce^{4+} and Ce^{3+} ions is reduced. This implies that the low formation energy of oxygen vacancies can reduce the thermodynamic barrier of the transition from $Ce^{4+} \rightarrow Ce^{3+}$. The transition from $Ce^{4+} \rightarrow Ce^{3+}$ arises from one oxygen atom escaping from the lattice, leaving one oxygen vacancy and two electrons. The two electrons are respectively trapped by two Ce^{4+} ions, causing the formation of two Ce^{3+} ions. The mesoporous ceria nanotubes have high oxygen storage capability. The existence of a large number of Ce^{3+} ions leads to the conversion of $O_2 \rightarrow O_2^-$. The active oxygen species (O_2^-) existing on the surface of ceria nanotubes causes high activity of $CO \rightarrow CO_2$ through combination of CO and O^-. The lower thermodynamic barrier for the transition cycle of $Ce^{4+} \leftrightarrow Ce^{3+}$ causes the catalytic activity of mesoporous ceria nanotubes to remain stable.

3. Conclusion

In summary, mesoporous polycrystalline ceria nanotubes have been synthesized. The specific surface area reaches 109 $m^2\ g^{-1}$. Large numbers of oxygen vacancy clusters on the surfaces of ceria nanotubes assist the transition from $Ce^{4+} \rightarrow Ce^{3+}$. The concentration of Ce^{3+} ions on the surfaces of the ceria nanotubes is about 23% that of the total cerium ions. The Ce^{3+} ions produce a large number of active oxygen (O_2^-) species, which cause enhanced efficiency in converting CO to CO_2. The conversion starting temperature of CO to CO_2 with mesoporous ceria nanotubes is about 100 °C lower than that with commercial ceria (CeO_2) particles. The specific activity of mesoporous ceria nanotubes is 9 times as high as that of the commercial ceria particles. We experimentally demonstrated that mesoporous ceria nanotubes with abundant oxygen vacancies and single electron defects of Ce^{3+} ions are the effective route for enhancing catalyst activity, which is of significance to the economy of energy and environment security.

4. Experimental

Synthesis

The ZnO nanorods were fabricated as templates *via* the hydrothermal synthesis method.[29] 15 mL of 0.1 M L^{-1} zinc acetate alcoholic solution was mixed with 30 mL of 0.5 M L^{-1} NaOH alcoholic solution. After stirring for 30 min, the mixture was transferred to a Teflon-lined stainless steel autoclave with a volume of 60 mL and heated at 160 °C for 24 h. The deposition product was then taken out and washed using distilled water. As a result, the ZnO nanorods were obtained. The assemblies of mesoporous polycrystalline ceria nanoshells on the ZnO nanorods were prepared by the ultrasonic assisted successive ionic layer adsorption and reaction (SILAR) method, along with annealing treatment. The detailed procedure is as follows: 0.1 g ZnO nanorods were ultrasonically dispersed in a 5 mL alcoholic solution of sodium hydroxide (0.1 M L^{-1}) for 5 min, followed by centrifugal separation and purgation with anhydrous alcohol. Then the ZnO nanorods were further ultrasonically dispersed in a 5 mL alcoholic solution of cerium nitrate for 5 min, followed by centrifugal separation and purgation with anhydrous alcohol. The above process is referred to as one deposition cycle. To obtain the ideal ceria nanoshell covered ZnO nanorods, the above deposition cycle was repeated about 20 times. The deposition product was annealed at 500 °C for 30 min to get mesoporous polycrystalline ceria nanoshell covered ZnO nanorods. Then they were treated by 5 vol.% HNO_3 to remove the ZnO nanorod core and were purged in deionized water several times to obtain the final products. Characterization by several techniques proves that the finally obtained product is mesoporous ceria nanotubes.

Characterization

Phase identification was performed with a Philips X'Pert powder X-ray diffractometer (XRD) using Cu-Kα (0.15419 nm) radiation. Field emission scanning electron microscopy (FESEM, Sirion 200) was used to observe the morphologies. Transmission electron microscopy (TEM JEM-2010) was used to examine the microstructures. Energy dispersive X-ray (EDX, Inca Oxford) analysis was conducted to determine the element composition. High resolution X-ray photoelectron spectroscopy (XPS) measurements were performed on an ESCALAB 250. The positron lifetime spectra (PLS) were measured using a fast-slow coincidence system with a resolution of 220 ps. A 10 μ Ci ^{22}Na positron source was sandwiched between two pieces of identical samples. Each spectrum was fitted by Lifetime9 program[30] and the variance of fit is less than 1.06. The broadening Doppler spectrum of the annihilation radiation was measured with a high pure germanium detector as a function of the incident positron energy; the measurement was performed at room temperature with a monoenergetic positron beam at Beijing ^{22}Na Slow Positron system.

Catalytic activity measurement

The catalytic activity measurements were conducted at atmospheric pressure in a continuous flow fixed-bed quartz tubular reactor. The reactant gas mixture consists 1.0% CO, 16% O_2, balanced with nitrogen. Gases were mixed by the mass flow controllers and directed through the quartz tubular reactor at the rate of 20 ml min^{-1}. The weight of catalyst was 0.03 g. All of the catalyst was filled in the middle of the quartz tubular reactor and heated in a ceramic furnace. Gases flowing through the quartz tubular reactor were monitored by gas chromatography. Temperature programmed reduction (H_2-TPR) experiments were carried out using a 10% H_2–N_2 mixture (40 mL min^{-1} flow rate) at a heating rate of 10 °C min^{-1}. 0.05 mg of catalyst was used. The catalyst was heated at 350 °C for 2 h and cooled to room temperature in Ar (30 mL min^{-1}) prior to the TPR experiment. The consumption of H_2 during the TPR experiment was measured by a thermal conductivity detector (TCD).

Acknowledgements

This work is financially supported by the National Major Project of Fundamental Research: Nanomaterials and Nanostructures (grant no. 2005CB623603). The authors would send their acknowledgement to Prof. Baoyi Wang and Weixin Huang for the helpful discussion and technical support.

References

1 J. C. Summers and S. A. Ausen, *J. Catal.*, 1979, **58**, 131.
2 E. P. Murray, T. Tsai and S. A. Barnett, *Nature*, 1999, **400**, 649.
3 T. Brezesinski, J. Wang, R. Senter, K. Brezesinski, B. Dunn and S. H. Tolbert, *ACS Nano*, 2010, **4**, 967.
4 J. P. Chen, S. Patil, S. Seal and J. F. McGinnis, *Nat. Nanotechnol.*, 2006, **1**, 142.
5 G. A. Silva, *Nat. Nanotechnol.*, 2006, **1**, 92.
6 C. Mandoli, F. Pagliari, S. Pagliari, G. Forte, P. D. Nardo, S. Licoccia and E. Traversa, *Adv. Funct. Mater.*, 2010, **20**, 1617.
7 X. Peng, Z. Luan, J. Ding, Z. Di, Y. Li and B. Tian, *Mater. Lett.*, 2005, **59**, 399.
8 Z. C. Di, J. Ding, X. J. Peng, Y. H. Li, Z. K. Luan and J. Liang, *Chemosphere*, 2006, **62**, 861.
9 B. Neltner, B. Peddie, A. Xu, W. Doenlen, K. Durand, D. S. Yun, S. Speakman, A. Peterson and A. Belcher, *ACS Nano*, 2010, **4**, 3227.
10 H. C. Yao and Y. F. Y. Yao, *J. Catal.*, 1984, **86**, 254.
11 I. Celardo, M. D. Nicola, C. Mandoli, J. Z. Pedersen, E. Traversa and L. Ghibelli, *ACS Nano*, 2011, **5**, 4537.
12 N. V. Skorodumova, S. I. Simak, B. I. Lundqvist, I. A. Abrikosov and B. Johansson, *Phys. Rev. Lett.*, 2002, **89**, 166601.
13 M. V. Ganduglia-Pirovano, A. Hofmann and J. Sauer, *Surf. Sci. Rep.*, 2007, **62**, 219.
14 M. M. Branda, C. Loschen, K. M. Neyman and F. Illas, *J. Phys. Chem. C*, 2008, **112**, 17643.
15 D. C. Sayle, X. Feng, Y. Ding, Z. L. Wang and T. X. T. Sayle, *J. Am. Chem. Soc.*, 2007, **129**, 7924.
16 P. Martin, S. C. Parker, D. C. Sayle and G. W. Watson, *Nano Lett.*, 2007, **7**, 543.
17 A. Trovarelli, *Catal. Rev. Sci. Eng.*, 1996, **38**, 439.
18 J. Guzman, S. Carrettin and A. Corma, *J. Am. Chem. Soc.*, 2005, **127**, 3286.
19 A. S. Deshpande, N. Pinna, B. Smarsly, M. Antonietti and M. Niederberger, *Small*, 2005, **1**, 313.
20 K. Zhou, X. Wang, X. Sun, Q. Peng and Y. Li, *J. Catal.*, 2005, **229**, 206.
21 K. Niesz and D. E. Morse, *Nano Today*, 2010, **5**, 99.
22 J. P. Holgado, R. Alvarez and G. Munuera, *Appl. Surf. Sci.*, 2000, **161**, 301.
23 R. K. Rehberg, H. S. Leipner, *Positron Annihilation in Semiconductros Defect Studies*, (Springer), 1998.
24 A. Sachdeva, S. V. Chavan, A. Goswami, A. K. Tyagi and P. K. Pujari, *J. Solid State Chem.*, 2005, **178**, 2062.
25 H. Norenberg and G. A. D. Briggs, *Phys. Rev. Lett.*, 1997, **79**, 4222.
26 F. Esch, S. Fabris, L. Zhou, T. Montini, C. Africh, P. Fornasiero, G. Comelli and R. Rosei, *Science*, 2005, **309**, 752.
27 D. M. Symth, *The defect chemistry of metal oxides*. Oxford University Press, 2000.
28 M. J. Puska and R. M. Nieminen, *Rev. Mod. Phys.*, 1994, **66**, 841.
29 B. Cheng and E. T. Samulski, *Chem. Commun.*, 2004, 986.
30 J. Kansy, *Nucl. Instrum. Methods Phys. Res., Sect. A*, 1996, **374**, 235.